

Title	Orthogonal chirp-division multiplexing for IM/DD-based short-reach systems
Authors	Ouyang, Xing;Talli, Giuseppe;Power, Mark;Townsend, Paul
Publication date	2019-08-02
Original Citation	Ouyang, X., Talli, G., Power, M. and Townsend, P. (2019) 'Orthogonal chirp-division multiplexing for IM/DD-based short-reach systems', Optics Express, 27(16), pp. 23620-23632. (12pp.) DOI: 10.1364/OE.27.023620
Type of publication	Article (peer-reviewed)
Link to publisher's version	https://www.osapublishing.org/oe/abstract.cfm?uri=oe-27-16-23620 - 10.1364/OE.27.023620
Rights	©2019 Optical Society of America under the terms of the OSA Open Access Publishing Agreement - https://doi.org/10.1364/OA_License_v1
Download date	2025-07-04 06:39:47
Item downloaded from	https://hdl.handle.net/10468/8596



UCC

University College Cork, Ireland
Coláiste na hOllscoile Corcaigh



Orthogonal chirp-division multiplexing for IM/DD-based short-reach systems

XING OUYANG,* GIUSEPPE TALLI, MARK POWER, AND PAUL TOWNSEND

Photonics Systems Group, Tyndall National Institute, University College Cork, Lee Maltings, Dyke Parade, Cork T12 R5CP, Ireland

*xing.ouyang@tyndall.ie

Abstract: Orthogonal chirp-division multiplexing (OCDM) has been recently proposed as an attractive modulation technique for realizing high-speed coherent lightwave systems in virtue of its resilience against system impairments. However, the complex-valued OCDM signal is not directly viable for optical intensity modulation and direct detection (IM/DD) systems. In this paper, a double-sideband (DSB)-modulated OCDM scheme is proposed for short-reach, high-speed IM/DD systems. In the proposed scheme, the real-valued OCDM signal is generated by a simple digital up-conversion technique, which converts the complex-baseband signal to a passband to avoid the aliasing for DSB modulation. At the receiver, inverse operations revert the signal back to the baseband for demodulation. Experiments were carried out to validate the feasibility and advantages of the proposed scheme, and OCDM signals with data rates up to 174.5 Gbit/s were successfully demonstrated. The results confirm that the proposed IM/DD-OCDM system is more robust to impairments and thus achieves better performance than a discrete multi-tone system.

© 2019 Optical Society of America under the terms of the [OSA Open Access Publishing Agreement](#)

1. Introduction

Enabled by the advances in the ultra-high-speed electronics during the last two decades, digital signal processing (DSP) technology plays a central role in modern fiber-optic communications, as it substantially enhances the capacity of optical networks to meet the ever-increasing demand for high-speed Internet and data services [1]. These versatile DSP techniques realize spectrally efficient modulation and reliable signal recovery for various application scenarios, from rack-scale datacenter communications to intercontinental transmission links [2–5]. For example, enabled by DSP, orthogonal frequency-division multiplexing (OFDM) is an attractive digital modulation technique for coherent optical (CO) systems for long-haul transmission [6–8], and it exhibits better resilience against dispersion than its single-carrier counterpart [9]. Its baseband scheme, discrete multi-tone (DMT) modulation, also shows benefit as a potential candidate for short-reach systems based on intensity modulation and direct detection (IM/DD) [10–12].

Recently, orthogonal chirp-division multiplexing (OCDM) has been demonstrated as a promising modulation technique for realizing high-speed coherent lightwave systems [13,14]. In the OCDM system, a large group of linearly frequency-modulated waveforms, referred to as chirps, as shown in Fig. 1(b), are employed for high-speed modulation. Compared with the traditional chirp spread spectrum (CSS) technique, the linear chirps in OCDM are mutually orthogonal and can be transmitted in the same time period and bandwidth, as illustrated in Fig. 1(d), without any interference. The orthogonal chirps attain the maximum spectral efficiency in terms of the Nyquist signaling rate [15]. In contrast, as shown in Figs. 1(a) and 1(c), the subcarriers in OFDM overlap in time, and are orthogonal in the frequency domain. Compared with the narrowband subcarriers in OFDM, the OCDM signal inherits the spread-spectrum feature from CSS. As a result of spreading the information over the entire bandwidth, the OCDM signals are more robust to impairments, and exhibit superior performance compared to other modulation techniques, such as, OFDM [13–16].

Considering the advantages of OCDM, it is highly desirable to find ways to apply OCDM to optical IM/DD systems, which are indispensable for cost-sensitive applications, such as, optical access networks and datacenter communications [17–20]. In such scenarios, OCDM can offer superior performance by combating specific impairments inherent in IM/DD systems. For example, the OCDM signal is insensitive to impairments, such as, bandwidth limitation from the low-cost electronic components, and the chromatic-dispersion (CD)-induced power fading effect in the IM/DD systems [21]. However, OCDM cannot be directly applied to IM/DD systems. In OCDM, the chirps are required to be complex-valued to satisfy the orthogonality condition, while IM/DD system offers only one dimension for modulation, namely, the intensity of the optical carrier.

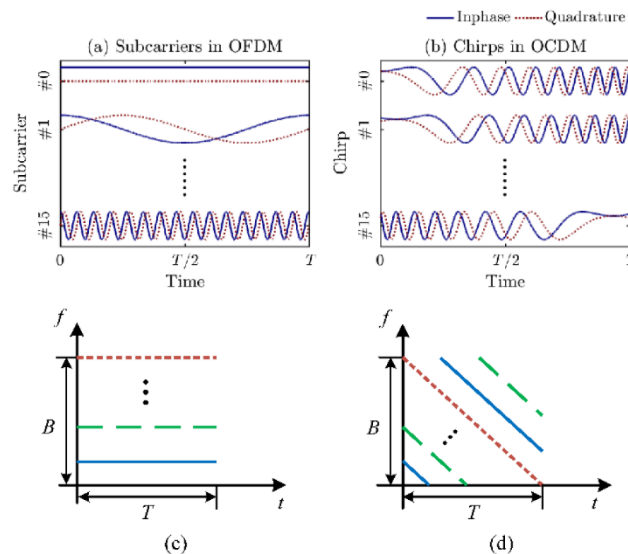


Fig. 1. Above: Waveforms for modulation: (a) a set of 16 subcarriers (harmonic series) in the OFDM and (b) a set of 16 chirps in the OCDM, where T denotes the period of an OFDM/OCDM symbol. Below: Illustration of Spectrograms of (c) OFDM signal and (d) OCDM signals.

In this paper, we propose a double-sideband (DSB) modulated OCDM scheme to realize high-speed IM/DD systems for short-reach applications [22]. In the proposed IM/DD-OCDM system, a digital up-conversion (DUC) technique converts the complex-baseband signal up to a passband. By doing so, the real part of the passband signal is equivalent to a DSB-modulated OCDM signal without aliasing, and is preserved for intensity modulation. The imaginary part is simply discarded. At the receiver, digital down-conversion (DDC) transforms the signal back to the baseband for demodulation. As the DUC and the DDC involve only phase rotations, only a trivial increase in complexity is required in the proposed IM/DD-OCDM system. Experiments were carried out to validate the feasibility and advantages of the proposed system, and IM/DD-OCDM signals with data rates up to 174.5 Gbit/s have been demonstrated. The results confirm that the proposed IM/DD-OCDM system is resilient to the impairments mentioned previously, and as a result outperforms a DMT-OFDM system.

The paper is organized as follows. In Section 2, the system model of the proposed IM/DD-OCDM is formulated in detail. Practical implementation and its advantages are also discussed. The experiment setup is provided in Section 3, and the results in Section 4. In the experiment, the DMT-OFDM was implemented for comparison. Section 5 discusses the advantages of the IM/DD-OCDM over DMT-OFDM. Finally, Section 6 concludes this paper.

2. System model of the IM/DD-OCDM system

In this section, the proposed IM/DD-OCDM system is formulated according to the linear time-invariant (LTI) model, and the block diagram of the proposed IM/DD-OCDM is shown in Fig. 2. To show its advantages, specific impairments, such as the CD-induced fading in the IM/DD systems are discussed analytically.

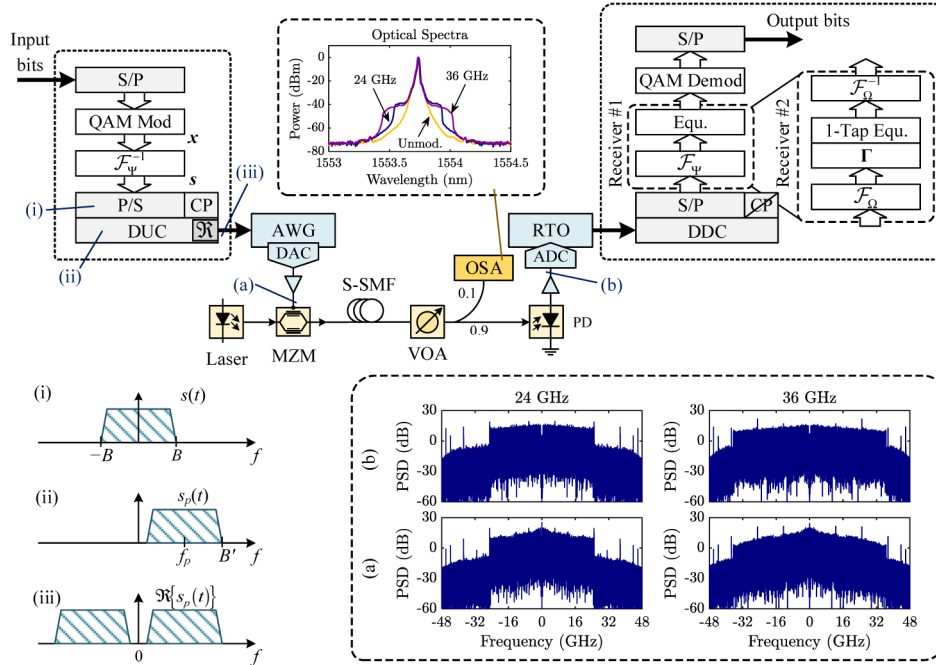


Fig. 2. System setup of the proposed IM/DD-OCDM system based on digital up-conversion. Insets: Illustration of the spectra of (i) the complex-baseband OCDM signal, (ii) the up-converted signal, and (iii) the real part of the up-converted signal. The measured electrical spectra of (a) transmitted signals and (b) received signals. Abbreviations: S/P: Serial-to-Parallel; P/S: Parallel-to-Serial; QAM: Quadrature Amplitude Modulation; DUC/DDC: Digital Up-/Down-Conversion; CP: Cyclic Prefix; AWG: Arbitrary Waveform Generator; RTO: Real-Time Oscilloscope; PD: Photodiode; DAC/ADC: Digital-to-Analog/Analog-to-Digital Converter. VOA: Variable Optical Attenuator.

2.1. Complex-baseband OCDM

The baseband OCDM transceiver is plotted in the dotted boxes in Fig. 2. The complex-baseband OCDM signal is a synthesis of a set of N mutually orthogonal chirps, $\psi_k(n)$, $k = 0, \dots, N - 1$, each of which is modulated by a symbol. In [13], we proved that the Fresnel transformation can synthesize the orthogonal chirps to generate OCDM signals, as

$$\begin{aligned}
 s(n) &= \mathcal{F}_\Psi^{-1}\{x(k)\}(n) = \sum_{k=0}^{N-1} x(k)\psi_k(n) \\
 &= \frac{1}{\sqrt{N}} e^{j\frac{\pi}{4}} \sum_{k=0}^{N-1} x(k) \times \begin{cases} e^{-j\frac{\pi}{N}(n-k)^2} & N \equiv 0 \pmod{2} \\ e^{-j\frac{\pi}{N}(n-k+\frac{1}{2})^2} & N \equiv 1 \pmod{2} \end{cases} \quad (1)
 \end{aligned}$$

where \mathcal{F}_Ψ is the discrete Fresnel transform (DFnT) and \mathcal{F}_Ψ^{-1} the inverse DFnT (DFnT), $x(k)$ is the symbol modulating the k -th chirp. It can be seen that in Eq. (1) the phase term of the

Fresnel transform is squared, which indicates that the chirps are essentially linear frequency modulated signals. The spectrogram of the OCDM is shown in Fig. 1(d), and discussion concerning OFDM and OCDM can be found in [13–15]. The complex-baseband OCDM signal can be efficiently generated by the fast algorithms for computing the DFNT [23]. Referring to Fig. 1, if an OCDM system has a bandwidth B , the length of an OCDM symbol is thus $T = N / B$ [14].

To avoid inter-symbol interference (ISI), guard interval (GI) should be inserted between the OCDM blocks. Based on the circular convolution property of DFNT, a cyclic prefix (CP) based GI maintains the circular convolution of OCDM signal through dispersive channels. Given that the impulse response of the system is $h(n)$, which characterizes the linear effects, such as the dispersion and filtering effects in the system, the received signal is

$$r(n) = h(n) \otimes s(n) + v(n), \quad (2)$$

where \otimes denotes the circular convolution operator, and $v(n)$ is the additive noise. In Eq. (2), the channel impulse response (CIR), $h(n)$, can model the linear dispersive effects in the system, such as filtering effects of the optical and electronic devices, and chromatic dispersion in the fiber. The noise term $v(n)$ represents the additive interference from the system, such as thermal noise from the electronics and amplified spontaneous emission noise in an optical amplifier.

In the initial proposal of OCDM [14], there are two types of baseband receiver schemes, as shown in the dotted box in Fig. 2. The first one is an intuitive method that directly transforms the received signal by a DFNT. By utilizing the convolution-preservation property of the DFNT, a time-domain equalizer or a frequency-domain equalizer (FDE) along with two discrete Fourier transforms (DFT) can then be used to compensate the channel. The second scheme exploits the eigen-decomposition of the DFNT to realize a more computationally efficient solution. In the second scheme, the received signal is transformed by a DFT instead of DFNT for the single-tap FDE. The signal can be then recovered by rotating the phases, Γ , which are actually the eigen-values of the DFNT with respect to DFT, and another IDFT. In Fig. 2, the differences of the two receiver schemes are indicated in the dashed boxes at the receiver end. In this paper, the second receiver algorithm is adopted due to its computational efficiency [14].

2.2. Proposed IM/DD-OCDM

It can be seen that the signal model is complex-valued in Eq. (1), and thus the baseband OCDM signal cannot be applied directly by modulating the optical intensity. To solve this problem, we proposed a DSB-modulated OCDM to realize IM/DD systems [22]. The basic principle of the proposed scheme is to convert the complex-baseband OCDM signal up to a passband so that all the spectral contents are located in positive frequencies. The real part of the passband signal is equivalent to a DSB-modulated signal. It preserves the entire information of the baseband signal, and thus can be used directly by modulating the intensity of an optical carrier.

Given that the continuous-time signal is $s(t)$, whose spectrum is shown in Fig. 2(i), the up-converted signal is thus

$$s_p(t) = e^{j2\pi f_p t} s(t), \quad (3)$$

where f_p is the frequency of the up-conversion carrier. The real-part of the up-converted signal can be accordingly given as

$$\begin{aligned} s_{\Re}(t) &= \Re\{s_p(t)\} \\ &= s_I(t) \cdot \cos 2\pi f_p t - s_Q(t) \cdot \sin 2\pi f_p t, \end{aligned} \quad (4)$$

where $s_I(t)$ and $s_Q(t)$ are the inphase and quadrature components of the complex-baseband signal $s(t)$. Applying the Fourier transform on Eq. (4), one can obtain

$$\begin{aligned} S_{\Re}(f) &= \mathcal{F}_p \{s_{\Re}(t)\} \\ &= \frac{1}{2} [S(f - f_p) + S^*(f + f_p)]. \end{aligned} \quad (5)$$

In Eq. (5), the real part of the signal $s_{\Re}(t)$ is in fact the DSB modulated signal, whose spectrum is shown in Fig. 2(iii). In Figs. 2(i)–2(iii), if the complex baseband bandwidth of the OCDM signal is B , and the up-conversion frequency f_p , the signal bandwidth after DUC is thus $B' = f_p + B$. In addition, it can be inferred that as long as the frequency f_p is larger than the bandwidth of the baseband signal, the real part of $s_p(t)$ preserves all the information of the baseband signal $s(t)$. Otherwise, aliasing occurs if $f_p < B$.

At the receiver, an inverse operation, i.e., digital down-conversion transforms the received signal back to the baseband for demodulation. As discussed in Section 2.1, the second receiver is adopted due to its superior efficiency. Referring to the receiver end in Fig. 2, the complex-baseband signal is transformed by a DFT, as

$$\begin{aligned} y(m) &= \mathcal{F}_{\Omega} \{r(n)\}(m) \\ &= H(m) \times \mathcal{F}_{\Omega} \{s(n)\}(m) + v_{\Omega}(m), \end{aligned} \quad (6)$$

where \mathcal{F}_{Ω} is the DFT operator, $H(m)$ is the channel frequency response (CFR), and $v_{\Omega}(m)$ is the noise in the frequency domain. With the eigen-decomposition property of the DFT,

$$\mathcal{F}_{\Omega} \{ \mathcal{F}_{\Psi}^{-1} \{x(k)\} \}(m) = \Gamma^*(m) \times \mathcal{F}_{\Omega} \{x(k)\}(m), \quad (7)$$

Equation (6) can be further given as

$$y(m) = H(m) \Gamma^*(m) \times \mathcal{F}_{\Omega} \{x(k)\}(m) + v_{\Omega}(m), \quad (8)$$

where $\Gamma(m)$ is the eigenvalue of DFNT w.r.t DFT. It can be seen that, except for a phase rotation $\Gamma^*(m)$, $y(m)$ is the DFT of $x(k)$ distorted by the CFR $H(m)$. The transmitted symbols can be recovered by single-tap equalizers, which compensate the dispersion $H(m)$ and phase rotation $\Gamma(m)$. Another IDFT is used to recover the transmitted symbols. For instance, if a zero-forcing equalizer is used, the estimated symbols are

$$\begin{aligned} \hat{x}(k) &= \mathcal{F}_{\Omega}^{-1} \{ H^{-1}(m) \Gamma(m) \times y(m) \}(k) \\ &= x(k) + \hat{v}(k), \end{aligned} \quad (9)$$

where $\hat{v}(k)$ is the noise after equalization.

In the proposed IM/DD-OCDM, there are one DUC and one DDC added to the traditional OCDM transceiver. Since these are implemented in the digital domain and only phase rotations are required with trivial arithmetic operations, the proposed scheme is simple to implement with only a minor increase in complexity. It should be noted that according to the Nyquist sampling theorem, the passband signal should be oversampled by a frequency of at least two times the bandwidth of the signal to avoid aliasing in Eq. (5). That is, the sampling rate should be larger than $2B'$, as indicated in Fig. 2(iii).

2.3. Chromatic-dispersion-induced fading effect

Inspecting Eqs. (2) and (6), the CIR or CFR function, namely $h(n)$ or $H(k)$ can characterize not only the CD effects in the fiber, but also other linear effects in the system, such as, electric and optical filters and amplifiers. In the IM/DD systems, CD in the fiber is the major

limiting factor by imposing severe fading effect in the high frequency region. The transfer function of the CD induced fading in the IM/DD systems [21] is given by

$$H_{\text{CD}}(f) \propto \cos(2\pi^2\beta_2 f^2 z), \quad (10)$$

where β_2 is the group velocity dispersion (GVD) parameter, and z is the distance along the fiber. It can be seen that the first null point, in Eq. (10) is inversely proportion to the fiber distance z and the square of the bandwidth. In other words, if we double the system bandwidth to double the data rate, the reach of a system will be reduced to one quarter.

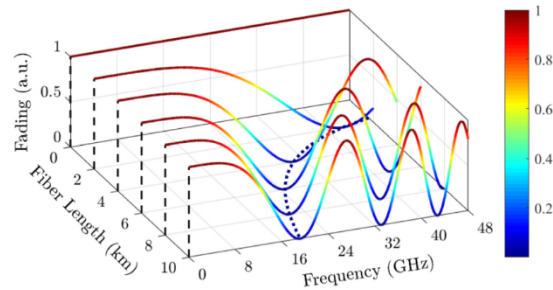


Fig. 3. Chromatic-dispersion-induced power fading effect in an IM/DD system with standard single-mode fiber at a wavelength of 1550 nm. The dotted line is the first frequency nulls of the fading over distance.

Figure 3 illustrates the CD-induced fading effect, which is the transfer function of a standard SMF (S-SMF) with a dispersion parameter of $D = 17$ ps/(nm·km) at 1550 nm. For example, at 2 km, the first null occurs at 42 GHz, and it reduces to 29.5 GHz at 4 km and 21 GHz at 8 km, respectively. For a practical system, the system should be operated to avoid the nulls from the signal. However, even if the system is well designed with sufficient redundancy such that no frequency notches occur within the bandwidth of the signal, the high-frequency components will still be degraded. For example, if we have an OFDM signal with a bandwidth of 30 GHz transmitted over 4 km, the subcarriers at a frequency greater than 20 GHz will experience severe fading with a power loss larger than 0.5 due to CD. On the other hand, the chirps in OCDM can spread the information over the entire bandwidth, and the information is still recoverable. To confirm this advantage, experiments were carried out, the results of which are shown in the following sections.

3. Experimental setup

Figure 2 details the experimental setup used to study the proposed IM/DD-OCDM system. At the transmitter, the signal was generated offline based on the model in Section II, and downloaded to an arbitrary waveform generator (AWG) with a 96-GSa/s digital-to-analog converter (DAC). The laser wavelength was at 1553.75 nm and the output power was 15 dBm. The Mach-Zehnder modulator (MZM) had a V_π of ~ 5 V and 32-GHz bandwidth, with an insertion loss of about 6 dB. The MZM was biased at its quadrature point, and the output power of the MZM was about 6 dBm. The electrical signal was amplified to a V_{pp} of 3.5 V to ensure the MZM was operated within its quasi-linear region. In this experiment, S-SMF with a length up to 4 km is adopted.

At the receiver, no optical amplifier was used to emulate short-reach scenarios. A variable optical attenuator (Agilent 8163B) followed by a 10:90 splitter was used to control and measure the input power to the photodiode (PD). The 10% port was connected to an optical spectrum analyzer (OSA), and the other 90% port to the PD, which was followed by an electrical amplifier (EA). A real-time oscilloscope (RTO) with a 200-GSa/s ADC sampled the signal for offline processing. Before demodulation, the signal was resampled to 96 GSa/s to match the sampling rate at the transmitter.

In the experiment, both the proposed IM/DD-OCDM and the conventional DMT-OFDM were implemented for comparison. In both systems, quadrature amplitude modulation (QAM) was adopted. Two setups were considered with signal bandwidths of (a) 24 and (b) 36 GHz, respectively, with corresponding Baud rates as 24 GBaud and 36 GBaud. In the case of 24 GHz, a highest data rate of 140 Gbit/s was attained with 64-QAM including the GI, and in the case of 36 GHz, 174.5 Gbit/s was achieved with 32-QAM. In the IM/DD-OCDM, there were 512 (768) chirps for modulation, and the time-domain signal was up-sampled to 2048 points per block. Equivalently, the oversampling ratio was 4 (8/3), and the complex-baseband signal had a bandwidth of 24 (36) GHz. The carrier frequency for DUC was 12.56 (18.56) GHz. For a fair comparison, in the DMT-OFDM system, there were 2048 subcarriers, of which the first 12 positive sub-carriers were nulls to avoid AC coupling and the following positive 512 (768) subcarriers were for payload. The remaining subcarriers were set to be nulls for the purpose of oversampling. Thus, the OFDM signal also had an effective oversampling ratio of 4 (8/3). To generate the real-valued DMT signal, the negative subcarriers were the complex-conjugate of their positive symmetries. In both systems, the length of CP was 64 points, with 3% overhead. Therefore, the length of an OFDM/OCDM symbol is 21.3 ns (22 ns including GI). The effective data rates were up to 140 Gbit/s for the 24 GHz signal with 64-QAM and 174.5 Gbit/s for the 36 GHz signal with 32-QAM, respectively. It should be noted that both systems were open loop without feedback from the receiver to the transmitter. Thus, no pre-emphasis was adopted. In addition, in this work, we adopted the super FEC scheme with a FEC limit at $\text{BER} = 3.8 \times 10^{-3}$ with 7% overhead as the benchmark for our experiments. This super FEC can achieve good performance and its cost and power consumption is acceptable in short-reach applications due to its relatively low decoding complexity.

4. Experimental results

In this section, to investigate the advantages of the proposed IM/DD-OCDM, the channel state information (CSI) of the system was first characterized, including the CIR and CFR, as well as the CD-induced fading effect in the fiber. Depending on the system status, experiments were carried out to realize the 140-Gbit/s OCDM signal over 4-km S-SMF and the 174.5-Gbit/s signal over a piece of short fiber of several meters in length.

4.1. Characterization of CSI

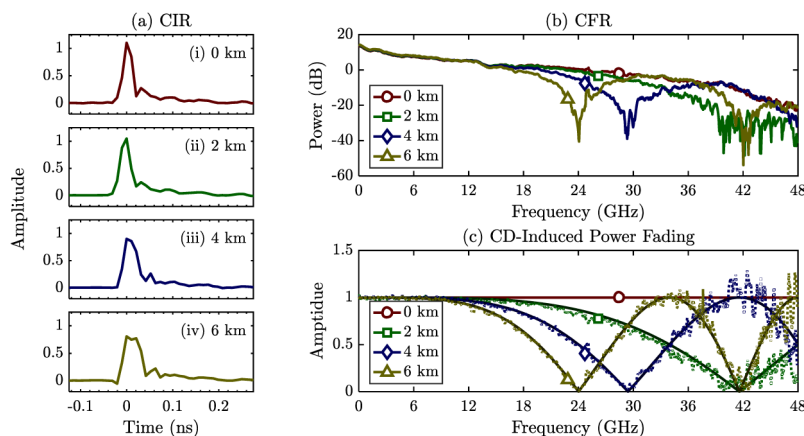


Fig. 4. Measured channel state information. (a) The channel impulse responses (CIRs) at (i) 0, (ii) 2, (iii) 4, and (iv) 6 km, respectively, and (b) the corresponding channel frequency response (CFR) of the system; (c) the measured (dotted lines) and theoretical (solid lines) chromatic dispersion (CD) induced power fading.

To study the effects of system impairments, Fig. 4 shows the measured CSI of the system at different fiber lengths, from 0 to 6 km. In Fig. 4(a), the CIR function is measured. As the fiber length increases, the CIR function begins to spread due to the increase of chromatic dispersion in the fiber. It can be seen that the pulse broadening is around 0.1 ns, which is equivalent to around 10 samples with a sampling rate of 96 GSa/s, and a GI length of 64 is sufficient to avoid the ISI between the symbol blocks in both OCDM and OFDM systems.

The corresponding CFR functions are provided in Fig. 4(b). It can be seen that the fading effect due to CD is more intuitive in the frequency domain. As the fiber length increases from 0 to 6 km, frequency notches, down to -60 dB, occur in the high frequency region. Signals will be severely degraded if operated in the vicinity of these notches. In Fig. 4(c), the CD-induced fading effects of the fiber link are measured and plotted by dotted lines. The analytical CD-induced fading effect based on Eq. (10) is plotted by the solid lines with a dispersion of $D = 17$ ps/(nm·km). It can be seen that the first frequency nulls due to CD occur at around 42 GHz and 29.5 GHz at 2 km and 4 km, respectively, with further reduction to 24 GHz at 6 km. In the experiment, based on the CSI characterization, we chose a fiber up to 4 km with a 24-GHz bandwidth signal.

4.2. BER performance of open-loop system

In Fig. 5, the bit-error rate (BER) performance of the 24-GHz signal of both OCDM and OFDM systems was measured against the received optical power. The data rates were 46.5, 93 and 140 Gbit/s for 4, 16 and 64-QAM, respectively. It can be seen that in all the cases in Figs. 5(a)–5(c), the proposed IM/DD-OCDM system always outperforms the DMT-OFDM system. In Fig. 5(a) with 4-QAM, the OCDM has only minor improvement over the OFDM without fiber transmission, since in the B2B case, there are only minor impairments without chromatic dispersion. As the fiber length increases, the improvement becomes more obvious. At a distance of 2 km, the required optical power for the OCDM signal is 1.5 dB less than the OFDM signal to attain a $\text{BER} = 10^{-6}$, and it increases to about 3.5 dB at 4 km. This improvement is because CD starts to degrade the system after fiber transmission, and OCDM exhibits better resilience to the CD than OFDM.

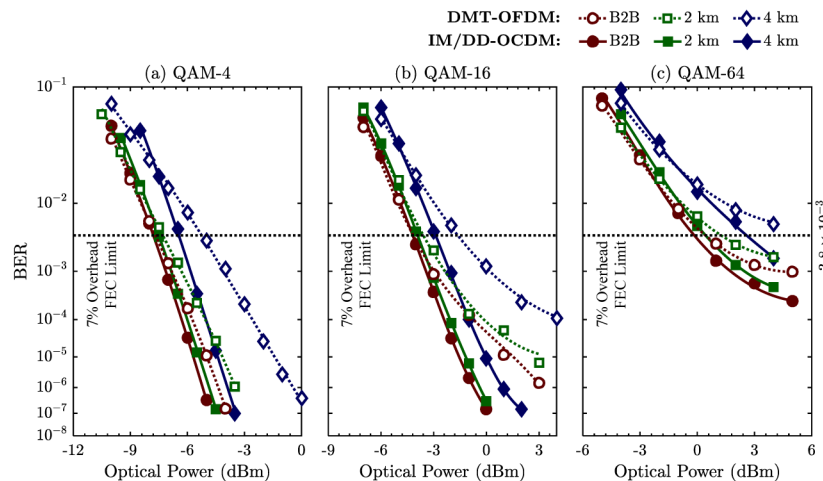


Fig. 5. Measured BER performance versus received optical power of the proposed IM/DD-OCDM and DMT systems with 24-GHz bandwidth: (a) QAM-4, (b) QAM-16, and (c) QAM-64.

The advantage of the OCDM signal is more obvious for high modulation levels, such as the 16 and 64-QAM in Figs. 5(b) and 5(c). For 16-QAM, the OCDM signal needs about 5.5 dB less received optical power than the OFDM signal at a $\text{BER} = 10^{-4}$. For 64-QAM, due to

the signal-to-noise (SNR) limitation of the optical transceiver, error floors occur in both systems even in the B2B case. Nonetheless, the OCDM signal has lower error floors than the OFDM signal. For example, the proposed IM/DD-OCDM system at 4 km attains a BER lower than 3.8×10^{-3} , the forward error correction (FEC) limit with 7% overhead, while the DMT-OFDM system cannot attain a BER below that limit.

In Fig. 6, the constellation diagrams of the received signals are provided. The received OFDM signal spreads as the fiber length increases from 0 to 4 km, with the 16-QAM signal at 4 km degrading to a BER = 1×10^{-3} , as indicated in Fig. 5(b). In contrast, the OCDM signal is less sensitive to the impairments, and the constellations remain more tightly clustered even after 4-km fiber.

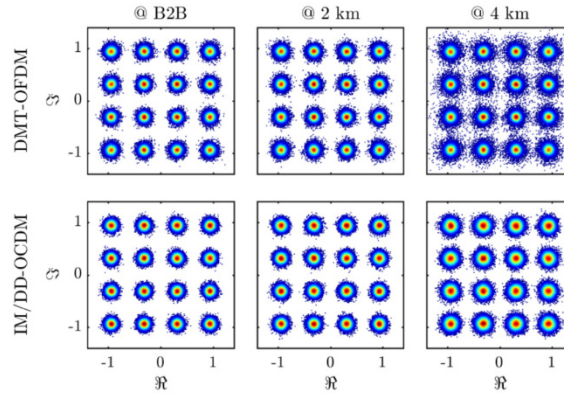


Fig. 6. The received constellation diagrams of QAM-16 signals of both systems with a received optical power at 0 dBm.

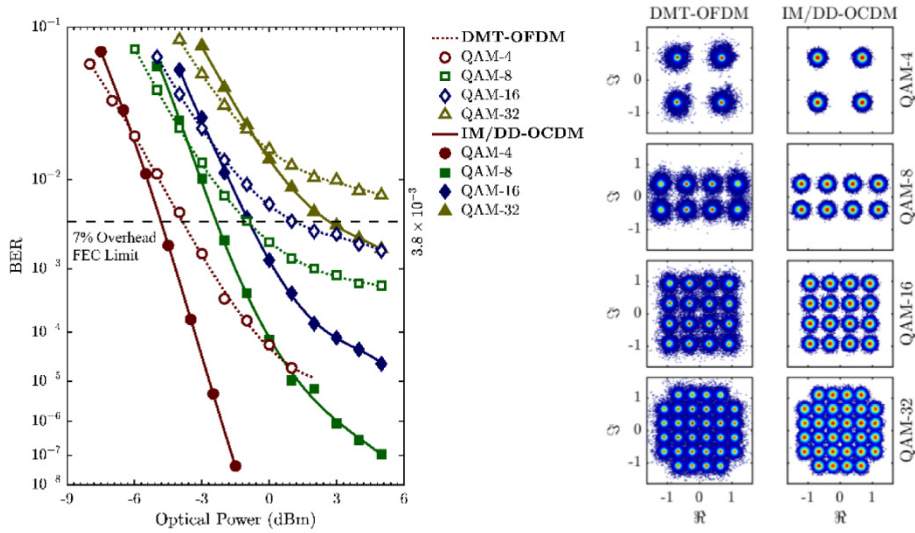


Fig. 7. (Left) Measured BER performance versus received optical power of the proposed IM/DD-OCDM and DMT-OFDM systems with 36-GHz bandwidth. (Right) The received constellation diagrams of various modulation levels of both systems with a received optical power at 3 dBm.

In Fig. 7, the bandwidth is increased to 36 GHz, and the data rate hits 174.5 Gbit/s with 32-QAM. Both systems exhibit similar performance trend as that in Fig. 5, while the performance difference is more obvious. For example, with a received optical power at 3 dBm, the proposed IM/DD-OCDM system can attain BER = 1×10^{-6} , 1×10^{-4} , and 3×10^{-3}

for 8, 16, and 32-QAM, respectively. In contrast, the DMT-OFDM has $\text{BER} = 1 \times 10^{-3}$, 3×10^{-3} , and 1×10^{-2} , respectively. In the case of 32-QAM, the OFDM signal cannot attain a BER lower than the FEC limit. On the right of Fig. 7, the received constellation diagrams of different modulation levels are shown for a received optical power of 3 dBm. It can be seen that even in B2B transmission, due to the impairments in the transceiver, the OFDM signals are much noisier than the OCDM signals, as discussed in the following.

4.3. Analysis

To investigate the performance differences between the OFDM and OCDM systems, the signal quality of the subcarriers in OFDM and chirps in OCDM are measured in terms of SNR. In Figs. 8(a) and (b), the quality of 24-GHz signal is measured at various distances. As the length of fiber increases, the performance of the high frequency OFDM subcarriers start to degrade, and SNR degradations as high as 7 dB can be observed. This is because in OFDM systems, information is conveyed in parallel in the frequency domain, and the high-frequency subcarriers are more susceptible to the CD-induced fading. In contrast, in OCDM systems, the information on each chirp is spread over the entire bandwidth as shown in Figs. 1(b) and (d). Hence, the information can be still recoverable with the presence of impairments, such as clock leakage and fading due to chromatic dispersion. Thus, the chirps in OCDM are insensitive to those impairments, and have flat SNRs with only minor degradation observed. The degradation in OCDM at 4 km is less than 3 dB in comparison the B2B case.

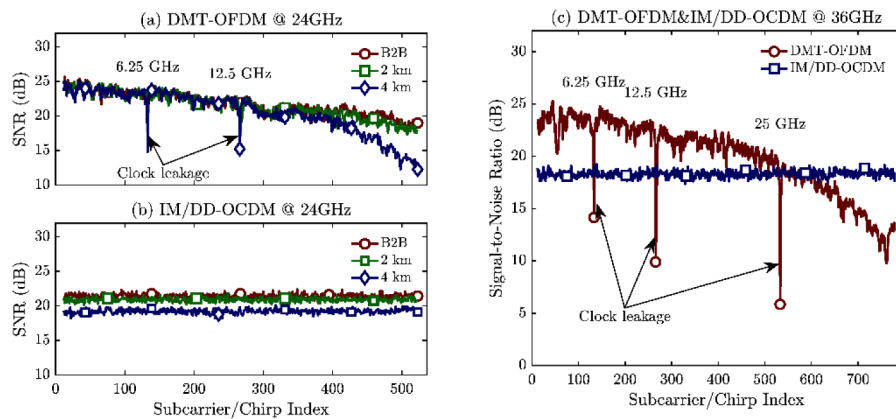


Fig. 8. The measured SNR of (a) the subcarriers in OFDM and (b) the chirps in OCDM with 24-GHz bandwidth at different distances, and (c) the measured SNR of both OFDM and OCDM with 36-GHz bandwidth at B2B.

The effect of these impairments become more severe if the signal bandwidth is increased to 36 GHz, as shown in Fig. 8(c). The bandwidth limitation of the opto-electronic components is more obvious. For reference, in the experiment, the MZM had a bandwidth of ~ 32 GHz. As the signal approaches the limit of the optoelectronic components, in the OFDM system, the edge subcarriers have an SNR as low as 10 dB. These effects account for the degradation of OFDM signal in Fig. 7. In contrast, the SNR of the chirps in OCDM is almost flat at about 18 dB and thus the system performance is superior to that of OFDM. In addition, it can be seen that, three low-SNR spikes occur at 6.25 and 12.5 GHz and 25 GHz, which are caused by the clock leakage from the high-speed DAC. In many short-reach applications, such as, PONs and datacenter communications, the systems operate in the O-band, where reduced CD allows longer distances for the optical links. In such systems, although CD imposes less fading effect than in the L-band, OCDM relaxes the stringent requirement on the high-speed optoelectronic devices, and consequently lower the system cost to achieve higher data rates.

4.4. BER performance of closed-loop system

We have shown in previous subsection that in an open-loop system, the proposed OCDM system outperforms the OFDM system due to its greater resilience to the system impairments. However if the additional complexity of a closed-loop system is acceptable, then the transmitter can be provided with knowledge of the channel state information. Adaptive modulation can be adopted to pre-compensate the impairments at the transmitter in order to improve the quality of the received signal. In this subsection, by feeding the CSI measured at the receiver back to the transmitter, pre-emphasis is applied. In the experiment, only the 36-GHz setup with 32-QAM was adopted and other parts of the system remained unchanged. Considering that the CD severely degrades the system in the L-band, as shown in Fig. 4, and that short-reach applications, such as, PONs and datacenter communications, usually operate in the O-band, in this section, a 1.5-km dispersion-shifted SMF is adopted to emulate the level of CD in O-Band transmission, whilst minimizing the change of the experimental setup. In the experiment, the water-pouring algorithm was employed to adapt the spectra of the transmitted signal and to ensure that the received spectral components had a flat SNR. In addition, as clock leakage was known to occur at certain frequencies, in the OFDM system, the subcarriers at these frequencies carried no data.

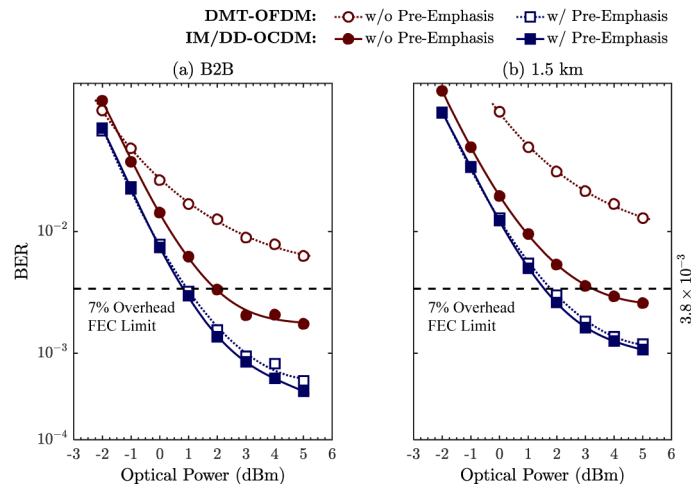


Fig. 9. Measured BER performance of both the proposed OCDM and OFDM systems with 36-GHz bandwidth and 32-QAM with the application of pre-emphasis algorithm. (a) B2B and (b) 1.5-km transmission.

In Fig. 9, the measured BER performance is provided. It can be seen that in Figs. 9(a) and 9(b), without the application of pre-emphasis, the performance of both systems is limited. For example, the OFDM system cannot attain a BER below the FEC limit, and the OCDM system has a BER just slightly below the FEC limit. If pre-emphasis is applied, obvious improvement is achieved for both systems. For example, in Fig. 9(a) without fiber transmission, both OFDM and OCDM have similar BERs $\approx 6 \times 10^{-4}$. In Fig. 9(b), slight degradation occurs with 1.5-km fiber transmission due to a small amount of chromatic dispersion from the dispersion shifted fiber. Nevertheless, with 5 dBm received optical power, both systems have a BER $\approx 1 \times 10^{-3}$, which is well below the FEC limit. In both Figs. 9(a) and 9(b), if pre-emphasis is applied, the proposed OCDM system only has minor improvement over OFDM because most impairments can be compensated with the CSI available at the transmitter end.

5. Discussion

In the experiments, both open-loop and closed-loop systems are considered to investigate the performance of both OFDM and OCDM. In the open-loop scheme, the transmitter has no knowledge about the CSI as there is no feedback from the receiver to the transmitter. Based on the experimental results, the proposed IM/DD-OCDM system outperforms the DMT-OFDM as the OCDM is insensitive to the impairments as discussed above. In a communication system with closed-loop feedback, the transmitter can have the entire or partial knowledge of the CSI, and pre-emphasis or adaptive modulation can be applied accordingly to counteract the fading effects and other impairments in the system. For instance, in Subsection 4.4, pre-emphasis is adopted. The power fading in the high frequency region can be compensated at the transmitter [24]. By doing this, the received signal can have a “flat” frequency response after transmission, avoiding the severe SNR degradation around the high frequency region.

However, to realize pre-emphasis or adaptive modulation, additional DSP hardware and a feedback link are required for implementing a closed-loop system. Specific algorithms are also required for coordinating the transceiver. In a practical optical system, the cost of deploying a feedback link may overwhelm the benefit gained, especially in the cost-sensitive short-reach systems. For example, in PONs which is a point-to-multipoint link, the reach of different optical network units is different. Pre-emphasis or adaptive modulation is usually infeasible in these systems. Therefore, for practical consideration, the proposed IM/DD-OCDM system is robust yet simple solution for high-speed short-reach systems. In addition, it has been shown in [25,26] that nonlinear equalizer based on the iterative block decision feedback equalization (IB-DFE) can effectively mitigate the power fading effect without the knowledge at the transmitter. In the IB-DFE algorithm, only the receiver acquires the CSI by channel estimation, and recover the corrupted information by compensate the distorted spectra due to fading effect [27].

6. Conclusions

In this paper, we propose and experimentally verify an OCDM scheme for high-speed IM/DD systems. In this scheme, the complex-baseband OCDM signal is up converted to a passband, and the real part, which is equivalent to DSB modulated signal, is preserved for modulating the optical intensity. At the receiver, an inverse operation transformed the signal back to baseband for demodulation. Experiments were implemented to realize the proposed system, and OCDM signal up to 174.5 Gbit/s has been demonstrated. The results show the proposed IM/DD-OCDM system exhibits better tolerance to impairment than the DMT-OFDM for its spread-spectrum nature of the OCDM signals. Considering the advantages of OCDM, the proposed system can serve an attractive candidate for short-reach applications, such as future high-speed PON and data-center communications.

Funding

Science Foundation Ireland (SFI) (12/IA/1270 and 12/RC/2276).

References

1. P. J. Winzer and D. T. Neilson, “From scaling disparities to integrated parallelism: A decathlon for a decade,” *J. Lightwave Technol.* **35**(5), 1099–1115 (2017).
2. M. Kuschnerov, F. N. Hauske, K. Piyawanno, B. Spinnler, M. S. Alfiad, A. Napoli, and B. Lankl, “DSP for coherent single-carrier receivers,” *J. Lightwave Technol.* **27**(16), 3614–3622 (2009).
3. E. M. Ip and J. M. Kahn, “Fiber impairment compensation using coherent detection and digital signal processing,” *J. Lightwave Technol.* **28**(4), 502–519 (2010).
4. P. J. Winzer, “High-spectral-efficiency optical modulation formats,” *J. Lightwave Technol.* **30**(24), 3824–3835 (2012).
5. K. Zhong, X. Zhou, J. Huo, C. Yu, C. Lu, and A. P. T. Lau, “Digital signal processing for short-reach optical communications: A review of current technologies and future trends,” *J. Lightwave Technol.* **36**(2), 377–400 (2018).

6. J. Armstrong, "OFDM for optical communications," *J. Lightwave Technol.* **27**(3), 189–204 (2009).
7. W. Shieh, H. Bao, and Y. Tang, "Coherent optical OFDM: theory and design," *Opt. Express* **16**(2), 841–859 (2008).
8. A. J. Lowery and L. B. Du, "Optical orthogonal division multiplexing for long haul optical communications: A review of the first five years," *Opt. Fiber Technol.* **17**(5), 421–438 (2011).
9. S. Beppu, K. Kasai, M. Yoshida, and M. Nakazawa, "2048 QAM (66 Gbit/s) single-carrier coherent optical transmission over 150 km with a potential SE of 15.3 bit/s/Hz," *Opt. Express* **23**(4), 4960–4969 (2015).
10. P. N. Ji, D. Qian, K. Kanonakis, C. Kachris, and I. Tomkos, "Design and evaluation of a flexible-bandwidth OFDM-based intra-data center interconnect," *IEEE J. Sel. Top. Quantum Electron.* **19**(2), 3700310 (2013).
11. N. Cvijetic, "OFDM for next-generation optical access networks," *J. Lightwave Technol.* **30**(4), 384–398 (2012).
12. S. Randel, F. Breyer, S. C. J. Lee, and J. W. Walewski, "Advanced modulation schemes for short-range optical communications," *IEEE J. Sel. Top. Quantum Electron.* **16**(5), 1280–1289 (2010).
13. X. Ouyang and J. Zhao, "Orthogonal chirp division multiplexing for coherent optical fiber communications," *J. Lightwave Technol.* **34**(18), 4376–4386 (2016).
14. X. Ouyang and J. Zhao, "Orthogonal chirp division multiplexing," *IEEE Trans. Commun.* **64**(9), 3946–3957 (2016).
15. X. Ouyang, O. A. Dobre, Y. L. Guan, and J. Zhao, "Chirp spread spectrum toward the Nyquist signaling rate — Orthogonality condition and applications," *IEEE Signal Process. Lett.* **24**(10), 1488–1492 (2017).
16. X. Ouyang, C. Antony, G. Talli, and P. D. Townsend, "Robust channel estimation for coherent optical orthogonal chirp-division multiplexing with pulse compression and noise rejection," *J. Lightwave Technol.* **36**(23), 5600–5610 (2018).
17. C. Kachris, K. Kanonakis, and I. Tomkos, "Optical interconnection networks in data centers: Recent trends and future challenges," *IEEE Commun. Mag.* **51**(9), 39–45 (2013).
18. J. C. Rasmussen, T. Takahara, T. Tanaka, Y. Kai, M. Nishihara, T. Drenski, L. Li, W. Yan, and Z. Tao, "Digital signal processing for short reach optical links," in *European Conference on Optical Communication* (IEEE, 2014), paper Tu.1.3.3.
19. D. Nessel, "NG-PON2 Technology and Standards," *J. Lightwave Technol.* **33**(5), 1136–1143 (2015).
20. R. Urata, H. Liu, X. Zhou, and A. Vahdat, "Datacenter interconnect and networking: from evolution to holistic revolution," in *Optical Fiber Communication Conference*, OSA Technical Digest (online) (Optical Society of America, 2017), paper W3G.1.
21. G. J. Meslener, "Chromatic dispersion induced distortion of modulated monochromatic light employing direct detection," *IEEE J. Quantum Electron.* **20**(10), 1208–1216 (1984).
22. X. Ouyang, G. Talli, M. Power, and P. Townsend, "Experimental demonstration of 112 Gbit/s orthogonal chirp-division multiplexing based on digital up-conversion for IM/DD systems with improved resilience to system impairments," in *European Conference on Optical Communication* (IEEE, 2018), paper Mo4F.3.
23. X. Ouyang, C. Antony, F. C. G. Gunning, H. Zhang, and Y. L. Guan, "Discrete Fresnel transform and its circular convolution property," arXiv:1510.00574 (2015).
24. D. Raffique, A. Napoli, S. Calabro, and B. Spinnler, "Digital preemphasis in optical communication systems: On the DAC requirements for terabit transmission applications," *J. Lightwave Technol.* **32**(19), 3247–3256 (2014).
25. X. Ouyang, G. Talli, and P. D. Townsend, "Iterative block decision feedback equalization for IM/DD-OCDM system to mitigate CD-induced fading," in *Conference on Lasers and Electro-Optics*, OSA Technical Digest (online) (Optical Society of America, 2019), paper SM3G.5.
26. X. Ouyang, G. Talli, M. Power, and P. D. Townsend, "Iterative block decision feedback equalization for IM/DD-based OCDM to compensate chromatic-dispersion-induced power fading," *J. Lightw. Technol.*, [www.doi.org/10.1109/JLT.2019.2923783](https://doi.org/10.1109/JLT.2019.2923783) (2019).
27. N. Benvenuto and S. Tomasin, "Iterative design and detection of a DFE in the frequency domain," *IEEE Trans. Commun.* **53**(11), 1867–1875 (2005).